This article has been accepted for publication in IEEE Transactions on Wireless Communications. This is the author's version which has not been fully edited and content may change prior to final publication. Citation information: DOI 10.1109/TWC.2024.3511579

Fluid Antenna Empowered Index Modulation for RIS-aided mmWave Transmissions

Jing Zhu, *Member, IEEE*, Qu Luo, *Member, IEEE*, Gaojie Chen, *Senior Member, IEEE*, Pei Xiao, *Senior Member, IEEE*, Yue Xiao, *Member, IEEE*, and Kai-Kit Wong, *Fellow, IEEE*

***Abstract*—In this paper, we propose a fluid antenna (FA) enabled joint transmit and receive index modulation (FA-JTR-IM) transmission mechanism for reconfigurable intelligent surface (RIS)-assisted millimeter-wave (mmWave) communication systems. By integrating the methodologies of FA and IM, the proposed scheme achieves enhanced spectral efficiency (SE) while requiring only a single radio frequency (RF) chain at both the transmitter and receiver. The proposed scheme offers a low hardware cost and power consumption transmission mechanism for the RIS-aided mmWave communication systems. Specifically, the encoding of information bits encompasses not only the modulated symbol but also the indices of transmit FA positions and receive antennas. To achieve a reliability-complexity trade-off, two types of detectors are introduced for the proposed FA-JTR-IM scheme, including the optimal maximum likelihood (ML) detector and two-step sequential (TSS) detector. Based on the ML detector, we derive the expression for the conditional pair-wise error probability of the proposed FA-JTR-IM scheme. Additionally, we provide the closed-form expressions for the unconditional PEP under the finite-path and infinite-path channel conditions, respectively. Simulation results demonstrate the superiority of the proposed FA-JTR-IM scheme in terms of error performance over its conventional benchmark schemes under the same SE condition.**

***Index Terms*—Reconfigurable intelligent surface, fluid antennas, index modulation, millimeter-wave, average bit error probability.**

I. INTRODUCTION

THE explosive growth in wireless communication demands has propelled the exploration of innovative solutions capable of meeting the stringent requirements of future networks. Among these, millimeter-wave (mmWave) communications have emerged as a promising candidate, owing to their vast available bandwidths and potential for high data rates [1], [2]. One of the notable limitation encountered in mmWave communication systems is the higher hardware cost and increased power consumption compared to conventional sub-6GHz systems [3]. This arises from the fact that mmWave systems often require massive multiple-input multiple-output (MIMO) with a high number of expensive radio frequency (RF) chains to enable beamforming, spatial multiplexing and diversity. Fluid antenna (FA) technique is considered as a promising solution to achieve enhanced spatial diversity with a lower hardware cost [4]–[6]. FA, also known as movable antenna (MA), has garnered significant interest in wireless communications due to its ability to dynamically adjust its position, shape, size, or radiation properties [4]. Compared to the conventional fixed position antenna (FPA) system, FA system has the capacity to fully leverage spatial diversity by dynamically adjusting the FA position within a defined finite region at the transceiver [5]–[7]. Existing research on FA system predominantly encompasses channel modeling, channel estimation, performance analysis and optimization. In detail, Wang *et al.* proposed the spatial correlation based channel model for the FA systems in [5], [6]. Subsequently, the field-response based channel model was proposed in [7], [8]. Then, channel estimation algorithms were explored for the spatial correlation channel model [9] and the field-response channel model [10]. Based on the aforementioned channel models, the methodology for antenna positioning design can be categorized into discrete port selection [11] and continuous position optimization [12], respectively. Moreover, the outage probability and diversity performance of the FA systems were derived in [13]–[15]. FA array enhanced beamforming has been investigated in [16]–[18]. The authors of [19] focused on optimizing beam coverage in FA arrays to enhance communication performance by dynamically adjusting weights and positions to suit varying conditions. More recently, the FA aided system was extended in wideband communication systems in [20].

On the other hand, index modulation (IM)-aided systems offer unique advantages, including high energy efficiency (EE), reduced hardware cost, and adaptable system architectures, which are achieved by introducing additional dimensions to convey information compared to conventional systems [21]–[23]. The incorporation of IM into traditional FPA frameworks exemplifies this paradigm shift. The concept of spatial modulation (SM) was explored in [24], wherein the utilization of the active antenna index introduces an extra dimension for transmitting information. In pursuit of enhanced spectral

---

This work was supported in part by the Fundamental Research Funds for the Central Universities, Sun Yat-sen University, under Grant 24hytd010 and in part by the U.K. Engineering and Physical Sciences Research Council under Grant EP/P03456X/1 and Grant EP/X013162/1. (Corresponding author: Gaojie Chen)

Jing Zhu and Gaojie Chen are affiliated with the School of Flexible Electronics (SoFE) & State Key Laboratory of Optoelectronic Materials and Technologies (OEMT), Sun Yat-sen University, Sun Yat-sen University, Shenzhen, Guangdong 518107, China (e-mail: ZJ009944@hotmail.com, gaojie.chen@ieee.org).

Qu Luo and Pei Xiao are affiliated with 5G and 6G Innovation Centre, Institute for Communication Systems (ICS) of University of Surrey, Guildford, GU2 7XH, UK (e-mail: {q.u.luo, p.xiao}@surrey.ac.uk).

Yue Xiao is affiliated with the National Key Laboratory of Wireless Communications, University of Electronic Science and Technology of China, Chengdu 611731, China (e-mail: xiaoyue@uestc.edu.cn)

Kai-Kit Wong is affiliated with the Department of Electronic and Electrical Engineering, University College London, Torrington Place, WC1E 7JE, United Kingdom and he is also affiliated with Yonsei Frontier Lab, Yonsei University, Seoul, Korea. (email: kai-kit.wong@ucl.ac.uk).

This article has been accepted for publication in IEEE Transactions on Wireless Communications. This is the author's version which has not been fully edited and content may change prior to final publication. Citation information: DOI 10.1109/TWC.2024.3511579

efficiency (SE) and reliability, a range of SM variants have been explored. These include generalized SM (GSM) [25], quadrature SM (QSM) [26], enhanced SM (ESM) [27], and receive SM (RSM) [28]. In [29], generalized beamspace modulation (GBM) was proposed for massive MIMO systems operating in mmWave spectrum, capitalizing on the unique attributes of mmWave massive MIMO technology.

Another limitation in mmWave communications is the susceptibility of mmWave signals to severe propagation losses and blockage, leading to unreliable connections and limited coverage areas [30]. To mitigate these challenges, researchers have turned their attention to novel technologies such as reconfigurable intelligent surfaces (RIS), which have demonstrated remarkable capabilities in enhancing signal propagation and coverage in mmWave environments [31]–[33]. RIS, composed of passive reflecting elements, can adaptively manipulate the electromagnetic waves incident upon them by controlling the phase shift of the reflected signals [34]. Through intelligent phase adjustment, RIS can effectively mitigate signal attenuation, exploit multi-path propagation, and enhance signal coverage, thus revolutionizing the design of mmWave communication systems. Recent research has focused on various aspects of RIS-aided mmWave communications, including channel modeling, channel estimation, beamforming design, and system optimization. In particular, the authors of [32] presented a novel model for outdoor-to-indoor communication empowered by RIS in mmWave networks. [33] proposed a channel estimation method based on atomic norm minimization for RIS-aided mmWave systems, facilitating accurate channel state information (CSI) acquisition. The integrated optimization of hybrid beamforming and reflection coefficients in RIS-aided mmWave systems were investigated in [35] and [36], aiming to maximize system performance. Additionally, the authors of [37] conducted ergodic achievable rate analysis and optimization for RIS-assisted mmWave communication systems, providing valuable guidelines for system design and resource allocation.

To address the challenges posed by mmWave communications, the integration of RIS with IM, RIS with FA as well as FA with IM has been explored in [38]–[43]. Specifically, the combination of RIS and IM has been investigated in [38]–[40]. The authors of [38] proposed a RIS-assisted spatial scattering modulation (SSM) scheme for mmWave communications, where a set of orthogonal paths are indexed to convey extra information bits. In [39], a novel cluster IM (CIM) transmission scheme was proposed for RIS-aided mmWave massive MIMO communications, offering enhanced system performance. Then, the authors of [40] investigated the RIS-enhanced mmWave communications with SM, where joint reflecting coefficients and hybrid beamforming optimization was conducted to further improve the error performance. Nonetheless, there is a paucity of research in the literature focusing on the integration of RIS-FA or FA-IM. Specifically, the authors of [41] proposed an RIS-assisted FA system, where the outage probability and delay outage rate performance were derived. A low-complexity beamforming design for RIS-assisted FA systems was proposed in [42]. The authors of [43] incorporated IM with FA-assisted MIMO systems to enhance the SE without additional hardware cost, where extra information bits are conveyed by indexing the FA positions. It is important to note that these works generally address individual issues in mmWave communications (i.e., using RIS to mitigate blockages, IM to improve spectral efficiency, or FA to achieve enhanced spatial diversity), rather than tackling multiple challenges simultaneously.

To the best of our knowledge, there is a lack of research focusing on the FA enabled IM for the RIS-assisted mmWave communications. The integration of FA, IM and RIS technologies is essential for reducing hardware costs, improving signal reliability in challenging mmWave environments, and enhancing SE through increased spatial diversity. This combination uniquely addresses the limitations of mmWave systems while maximizing performance without the need for additional complex hardware. In light of this gap, the primary contributions of this paper can be outlined as illustrated below.

- We devise a novel FA empowered joint transmit and receive index modulation (FA-JTR-IM) transmission scheme for RIS-aided mmWave single-input multiput-output (SIMO) communication systems, where both the transmit FA positions and the receive antennas are indexed to convey additional information bits. Hence, the proposed scheme yields elevated SE, while preserving the distinctive single-RF transceiver structure. Moreover, with the assistance of the RIS, the beamforming procedure in conventional JTR-IM can be substituted by adjusting the reflecting coefficients of the RIS elements.
- We propose a low-complexity detector, namely two-step sequential (TSS) detector, tailored to mitigate the computational complexity. Compared to the maximum likelihood (ML) detector, it strikes a good balance between complexity and detection accuracy. This proposed TSS detector commences with the estimation of the receive antenna index, followed by the employment of an optimal search algorithm to jointly identify the location index of the transmit FA and the modulated symbol.
- We analyze the error performance of the proposed scheme. To be specific, a detailed derivation of the conditional pair-wise error probability (CPEP) for the proposed scheme is performed based on the ML detection algorithm. Then, the closed-form expressions of unconditional PEP (UPEP) are obtained under the conditions of finite-path and infinite-path channels via the probability density function (PDF) method.
- We conduct Monte Carlo simulations to confirm the benefits of the proposed approach. The key findings are summarized as follows: 1) the accuracy of the theoretical analysis for average bit error probability (ABEP) is rigorously verified; 2) the proposed FA-JTR-IM scheme is superior to its relevant benchmark schemes; 3) the ML detector provides the best error performance, but the proposed TSS detector strikes a balance between error performance and computational complexity.

The following sections of this paper are organized as follows. Section II presents the channel model as well as the transceiver model of the proposed FA-JTR-IM scheme. Section

III provides the derivation for the ABEP performance is outlined. Section IV offers the simulation results to substantiate the effectiveness of the proposed system. Finally, Section V provides the concluding remarks of this paper.

Notations: $|\cdot|$ and $\|\mathbf{A}\|$ refer to the absolute value and the Frobenius norm, respectively. $(\cdot)^H$ and $(\cdot)^T$ are the Hermitian transpose and transpose, respectively. $\mathrm{diag}(\cdot)$ and $\mathbb{E}(\cdot)$ are the diagonal and expectation operation, respectively. $\Re\{\cdot\}$ represents the real part of a complex variable. $\mathbb{C}^{M\times N}$ denotes the space of $M\times N$ complex matrices. $\jmath$ refers to the imaginary unit, i.e., $\jmath^2=-1$. $Q(x)=\frac{1}{\sqrt{2\pi}}\int_x^{\infty}\exp(-u^2/2)\mathrm{d}u$ is the Gaussian Q-function. $\angle(x)$ represents the angle response of x. $\mathbf{I}_N$ refers to an N-dimensional identity matrix.

II. SYSTEM MODEL

In Fig. 1, we consider an RIS-assisted mmWave SIMO communication system, where the transmitter (Tx) is equipped with a single FA (i.e., $N_t=1$) and the receiver (Rx) has N_r fixed position antennas[1]. In the mmWave band, high penetration loss frequently causes blockages and outages [44]. Therefore, we assume that there is no direct link between the Tx to the Rx[2]. The deployment of RIS is designed to mitigate these challenges by improving the communication environment. As shown in Fig. 1, the transmit FA is connected to a single RF chain through flexible connectors such as coaxial cables. The entire FA transmission region is partitioned into $T=T_1\times T_2$ grids, where T_1 and T_2 are the number of grids along horizontal and vertical directions, respectively. In this study, it is assumed that the transmit FA possesses the capability to move freely within these T grids. The RIS is composed of a fixed uniform planar array (UPA) of size $N=N_1\times N_2$, where N_1 and N_2 are the number of UPA elements along horizontal and vertical directions, respectively. Similarly, the Rx is also composed of a fixed UPA of size $N_r=R_1\times R_2$, where R_1 and R_2 are the number of UPA elements along horizontal and vertical directions, respectively.

A. Channel Model

To begin with, we set up Cartesian coordinate systems to define the positions of the transmit FA, RIS as well as receive UPAs. The set of coordinates representing all the possible positions of the transmit FA is denoted as $\mathcal{T}=[\mathbf{t}_{1,1},\mathbf{t}_{1,2},...,\mathbf{t}_{m,n},...,\mathbf{t}_{T_1,T_2}]$, where $\mathbf{t}_{m,n}=[x_{\mathrm{t},m},y_{\mathrm{t},n}]$, $m=1,...,T_1$, $n=1,...,T_2$. The set of coordinates representing the receive UPA is denoted as $\mathcal{R}=[\mathbf{r}_{1,1},\mathbf{r}_{1,2},...,\mathbf{r}_{p,q},...,\mathbf{r}_{R_1,R_2}]$ with $\mathbf{r}_{p,q}=[x_{\mathrm{r},p},y_{\mathrm{r},q}]$, $p=1,...,R_1$, $q=1,...,R_2$. The set of coordinates representing the RIS is denoted as $\mathcal{N}=[\mathbf{n}_{1,1},\mathbf{n}_{1,2},...,\mathbf{n}_{u,v},...,\mathbf{n}_{N_1,N_2}]$ with $\mathbf{n}_{u,v}=[x_{\mathrm{R},u},y_{\mathrm{R},v}]$, $u=1,...,N_1$, $v=1,...,N_2$.

The RIS-assisted link can be represented as a combination of three components: the Tx-RIS link, RIS phase-shift matrix and RIS-Rx link. In this paper, we employ the widely recognized Saleh-Valenzuela (S-V) based field-response channel model for mmWave communications. In addition, we assume that the RIS is located close to the Tx to ensure a strong line-of-sight (LoS) connection between the Tx and RIS. Moreover, since the Rx is situated at a considerable distance from both the Tx and RIS, it is evident that the non-LoS (NLoS) propagation significantly influences the RIS-Rx link [2].

1) *Tx-RIS channel:* The channel between the Tx and RIS can be represented as

$$\mathbf{H}=[\mathbf{h}(\mathbf{t}_{1,1}),...,\mathbf{h}(\mathbf{t}_{m,n}),...,\mathbf{h}(\mathbf{t}_{T_1,T_2})]\in\mathbb{C}^{N\times T},\qquad(1)$$

where $\mathbf{h}(\mathbf{t}_{m,n})=\mathbf{b}^H\rho_{\mathrm{t}}(\mathbf{t}_{m,n})\in\mathbb{C}^{N\times 1}$ is the channel vector from the transmit FA situated at position $\mathbf{t}_{m,n}=[x_{\mathrm{t},m},y_{\mathrm{t},n}]$ to the RIS. Those terms are defined as

- $\mathbf{b}=[b(\mathbf{n}_{1,1}),...,b(\mathbf{n}_{u,v}),...,b(\mathbf{n}_{N_1,N_2})]\in\mathbb{C}^{1\times N}$ is the field-response vector (FRV) in the RIS region. $b(\mathbf{n}_{u,v})=\rho_{\mathrm{R}}(\mathbf{n}_{u,v})=e^{\jmath\frac{2\pi}{\lambda}(x_{\mathrm{R},u}\cos\theta_{\mathrm{R}}\sin\phi_{\mathrm{R}}+y_{\mathrm{R},v}\sin\theta_{\mathrm{R}})}$, where $\theta_{\mathrm{R}}\in[0,2\pi]$ and $\phi_{\mathrm{R}}\in[0,2\pi]$ are the elevation and azimuth angles, respectively, and λ is the wavelength.
- $\rho_{\mathrm{t}}(\mathbf{t}_{m,n})=e^{\jmath\frac{2\pi}{\lambda}(x_{\mathrm{t},m}\cos\theta_{\mathrm{t}}\sin\phi_{\mathrm{t}}+y_{\mathrm{t},n}\sin\theta_{\mathrm{t}})}$, $\theta_{\mathrm{t}}\in[0,2\pi]$ and $\phi_{\mathrm{t}}\in[0,2\pi]$ are the elevation and azimuth angles, respectively.

2) *RIS-Rx channel:* According to [8], the channel between the RIS and Rx can be expressed as

$$\mathbf{G}=[\mathbf{g}(\mathbf{r}_{1,1}),...,\mathbf{g}(\mathbf{r}_{p,q}),...,\mathbf{g}(\mathbf{r}_{R_1,R_2})]^T\in\mathbb{C}^{N_r\times N},\qquad(2)$$

where $\mathbf{g}(\mathbf{r}_{p,q})=\mathbf{F}^H\mathbf{\Xi}\mathbf{k}(\mathbf{r}_{p,q})\in\mathbb{C}^{N\times 1}$ is the channel vector between the RIS and receive UPA element located at position $\mathbf{r}_{p,q}=[r_{\mathrm{r},p},y_{\mathrm{r},q}]$. Specifically, the terms are defined as follows

- $\mathbf{F}=[\mathbf{f}(\mathbf{n}_{1,1}),...,\mathbf{f}(\mathbf{n}_{u,v}),...,\mathbf{f}(\mathbf{n}_{N_1,N_2})]\in\mathbb{C}^{L\times N}$, where L is the number of channel paths between the RIS and Rx and $\mathbf{f}(\mathbf{n}_{u,v})\in\mathbb{C}^{L\times 1}$ denotes the FRV of the RIS.
- $\mathbf{f}(\mathbf{n}_{u,v})=[\rho_{\mathrm{R},1}(\mathbf{n}_{u,v}),...,\rho_{\mathrm{R},l}(\mathbf{n}_{u,v}),...,\rho_{\mathrm{R},L}(\mathbf{n}_{u,v})]^T$, where $\rho_{\mathrm{R},l}(\mathbf{n}_{u,v})=e^{\jmath\frac{2\pi}{\lambda}(x_{\mathrm{R},u}\cos\theta_{\mathrm{R},l}\sin\phi_{\mathrm{R},l}+y_{\mathrm{R},v}\sin\theta_{\mathrm{R},l})}$, $\theta_{\mathrm{R},l}\in[0,2\pi]$ and $\phi_{\mathrm{R},l}\in[0,2\pi]$ are the elevation and azimuth angles of the lth path, respectively, for $l=1,...,L$.
- $\mathbf{\Xi}=\mathrm{diag}(\alpha_1,...,\alpha_l,...,\alpha_L)\in\mathbb{C}^{L\times L}$ is the path-response matrix (PRM) between the RIS and Rx, where $\alpha_l\sim\mathcal{CN}(0,c/L)$ with $c=c_0d^{-\varpi}$ represents the anticipated channel gain, c_0 denotes the unit distance path loss, d signifies the distance from the RIS to the Rx, and ϖ refers to the path loss exponent.
- $\mathbf{k}(\mathbf{r}_{p,q})=[\rho_{\mathrm{r},1}(\mathbf{r}_{p,q}),...,\rho_{\mathrm{r},l}(\mathbf{r}_{p,q}),...,\rho_{\mathrm{r},L}(\mathbf{r}_{p,q})]^T$, where $\rho_{\mathrm{r},l}(\mathbf{r}_{p,q})=e^{\jmath\frac{2\pi}{\lambda}(x_{\mathrm{r},p}\cos\theta_{\mathrm{r},l}\sin\phi_{\mathrm{r},l}+y_{\mathrm{r},q}\sin\theta_{\mathrm{r},l})}$, $\theta_{\mathrm{r},l}\in[0,2\pi]$ and $\phi_{\mathrm{r},l}\in[0,2\pi]$ are the elevation and azimuth angles of the lth path, respectively, for $l=1,...,L$.

3) *Composite channel:* The signal emitted from the Tx traverses the Tx-RIS-Rx channel before reaching the Rx. In essence, the RIS functions as a passive beamformer, reflecting the signal over a specific transmit FA position to a specific receive UPA element in the mmWave channel. Expressing ψ_τ as the phase shift corresponding to the τth passive RIS element, the vector of RIS reflection coefficients is given by

$$\mathbf{\Psi}=[e^{\jmath\psi_1},...,e^{\jmath\psi_\tau},...,e^{\jmath\psi_N}]\in\mathbb{C}^{N\times 1}.\qquad(3)$$

---

[1] It is worth mentioning that this work focuses on single-user scenarios to simplify the analysis and clearly illustrate the key principles of the proposed FA-JTR-IM scheme. However, the proposed transmission scheme can be extended to multi-user scenarios, which will be explored in the future work.

[2] The introduction of a direct link would increase system complexity, as we would need to dynamically manage both the direct link and the RIS-assisted link. This will be part of our future work.

This article has been accepted for publication in IEEE Transactions on Wireless Communications. This is the author's version which has not been fully edited and content may change prior to final publication. Citation information: DOI 10.1109/TWC.2024.3511579

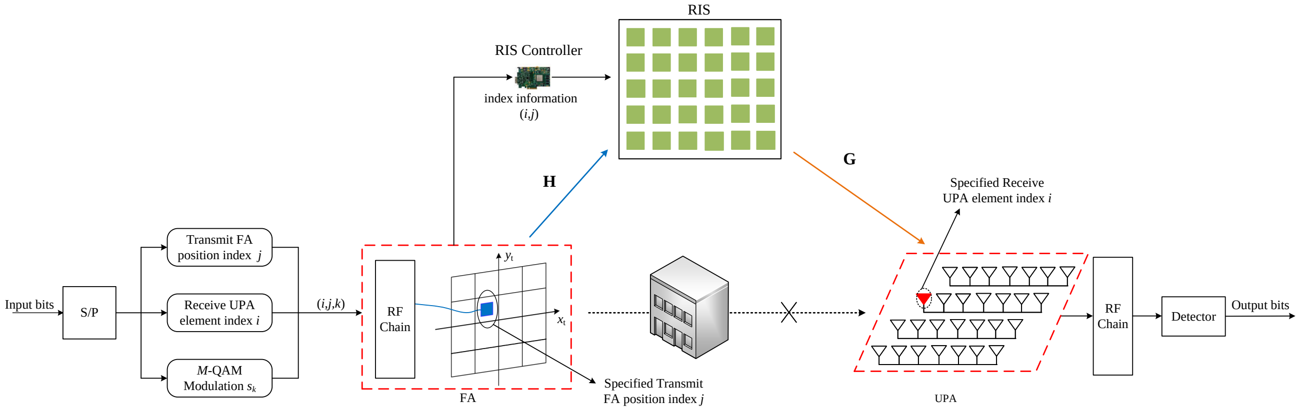

Fig. 1. Block diagram of the proposed FA-JTR-PIM system for RIS-aided mmWave Communications.

B. Proposed FA-JTR-IM Transmission

As illustrated in Fig. 1, the principle of IM is applied concurrently at the Tx and Rx ends, where the transmit FA region grids and the fixed receive UPA elements are meticulously indexed, respectively. In particular, only one of the T grids is utilized by the transmit FA for signal transmission, and one out of N_r receive UPA elements is selected to receive signal. In the proposed FA-JTR-IM scheme, the incoming bit stream is divided into three parts: 1) the first $\log_2(T)$ bits are used to select the jth $(j \in \{1, 2, ..., T\})$ transmit FA position index, which indicates that the position $\mathbf{t}_{m,n}$ is occupied by the single transmit FA. The relationship between the transmit FA position index j and the position coordinate (m, n) mapping process is given by $j = (m - 1)T_2 + n$, $m = 1, ..., T_1$ and $n = 1, ..., T_2$; 2) The next $\log_2 N_r$ bits are used to determine the receive UPA element index i $(i \in \{1, 2, ..., N_r\})$, where $i = (p-1)R_2+q$, $p = 1, ..., R_1$ and $q = 1, ..., R_2$; and 3) The remaining $\log_2(M)$ bits are modulated to an M-quadrature amplitude modulation (QAM) symbol s_k, $k \in \{1, 2, ..., M\}$.

In this work, we normalize the power incident upon the RIS to unity for ease of analysis [45]. It is important to note that this normalization does not imply any change to the actual transmit power constraints, which remain determined by the transmitter or source in accordance with system design. Thus, the signal received at the Rx is written as

$$\mathbf{y} = \sqrt{P}\mathbf{G}\mathrm{diag}(\mathbf{\Psi})\frac{\mathbf{H}\mathbf{e}_j}{\|\mathbf{H}\mathbf{e}_j\|_2}s_k + \mathbf{w}, \tag{4}$$

where $\mathbf{y} \in \mathbb{C}^{N_r\times 1}$ is the received signal, P is the transmit power, $\mathbf{w} \in \mathbb{C}^{N_r\times 1} \sim \mathcal{CN}(0, N_0\mathbf{I}_{N_r})$ is the additive white Gaussian noise (AWGN) and $\mathbf{e}_j$ is the jth column of identity matrix $\mathbf{I}_T$.

To obtain the maximum instantaneous signal-to-noise ratio (SNR) at the ith receive UPA element, the reflection coefficients should satisfy $\psi_\tau+\vartheta_{\tau j}+\varphi_{i\tau} = 0, \tau = 1, 2, ..., N$, where $\vartheta_{\tau j}$ and $\varphi_{i\tau}$ are the angle response of the Tx-RIS and RIS-Rx links, i.e., $\vartheta_{\tau j} \in \{\angle(\mathbf{H})\}$ and $\varphi_{i\tau} \in \{\angle(\mathbf{G})\}$, respectively. According to (1), $\|\mathbf{H}\mathbf{e}_j\|_2^2 = \|\mathbf{h}(\mathbf{t}_{m,n})\|_2^2 = N$. The received signal can thus be further written as

$$\mathbf{y} = \sqrt{\frac{P}{N}}\mathbf{G}\mathrm{diag}(\mathbf{\Psi}_{ij})\mathbf{H}\mathbf{e}_j s_k + \mathbf{w}. \tag{5}$$

C. Signal Detection

At the receiver, it is assumed that perfect CSI is available, while the impact of imperfect CSI will be addressed in Section IV. To seek a reliability-complexity tradeoff, two types of detectors are introduced in this subsection, which will be detailed in the sequel.

1) Optimal ML detector: The optimal ML detector is employed to simutaneously identify the active position of transmit FA, the receive UPA element, and the modulated symbol, which is given by

$$(\hat{i}, \hat{j}, \hat{k}) = \underset{i,j,k}{\arg\min} \left\|\mathbf{y} - \sqrt{\frac{P}{N}}\mathbf{G}\mathrm{diag}(\mathbf{\Psi}_{ij})\mathbf{H}\mathbf{e}_j s_k\right\|_2^2. \tag{6}$$

2) Low-complexity TSS detector: Given that the optimal ML detector necessitates exploring all 2^R possible combinations of (i, j, k), it leads to high computational complexity, especially when the transmission rate R is large. In response to this challenge, we introduce a low-complexity TSS detection algorithm and the detailed procedure is given as follows.

Step 1: First, by exploiting the maximized energy in a specific receive UPA element from the transmit FA with the assistance of RIS, the estimated active receive UPA element index $\hat{i}$ can be obtained as

$$\hat{i} = \underset{i\in\{1,2,...,N_r\}}{\arg\max} |\mathbf{y}(i)|^2. \tag{7}$$

Step 2: Assuming the receive UPA element index is detected correctly, the transmit FA position index j as well as the modulated symbol s_k can be jointly detected by

$$(\hat{j}, \hat{k}) = \underset{j\in\{1,..,T\},k\in\{1,...,M\}}{\arg\min} \left\|\mathbf{y} - \sqrt{\frac{P}{N}}\mathbf{G}\mathrm{diag}(\mathbf{\Psi}_{\hat{i}j})\mathbf{H}\mathbf{e}_j s_k\right\|_2^2. \tag{8}$$

3) Complexity Analysis: The computational complexity is delineated through real-valued flops, comprising both real-valued multiplications and additions. For the given matrices or vectors $\mathbf{A} \in \mathbb{C}^{m\times n}$, $\mathbf{B} \in \mathbb{C}^{n\times p}$, $\mathbf{a} \in \mathbb{C}^{n\times 1}$ and $\mathbf{b} \in \mathbb{C}^{n\times 1}$, the corresponding computational complexity is given as

$$\begin{aligned} C_{\mathbf{AB}} &= 2mp(4n-1) \\ C_{\mathbf{a}-\mathbf{b}} &= 4n-1 \\ C_{\|\mathbf{a}\|_2^2} &= 2n. \end{aligned} \tag{9}$$

This article has been accepted for publication in IEEE Transactions on Wireless Communications. This is the author's version which has not been fully edited and content may change prior to final publication. Citation information: DOI 10.1109/TWC.2024.3511579

TABLE I
THE COMPUTATIONAL COMPLEXITY COMPARISON OF DIFFERENT DETECTORS FOR THE FA-JTR-IM SCHEME

(N_r, N, T, M)	Detectors		Complexity reduction compared to ML
	Optimal ML	Proposed TSS	
(4,128,4,4)	3.4×10^7	8.6×10^6	75%
(16,16,16,4)	6.6×10^7	4.2×10^6	94%
(64,128,8,4)	1.8×10^{10}	2.8×10^8	98%

The computational complexity of the optimal ML detector can be calculated as

$$C_{\mathrm{ML}} = 2^R[2N_r(N+T)(4N-1)+6N_r], \tag{10}$$

where 2^R is the total search space of the proposed FA-JTR-IM scheme, and $2N_r(N+T)(4N-1)+6N_r$ is the complexity of calculating $\|\mathbf{y}-\sqrt{\frac{P}{N}}\mathbf{G}\mathrm{diag}(\mathbf{\Psi}_{ij})\mathbf{H}\mathbf{e}_j s_k\|_2^2$ in (6).

For the proposed TSS detection algorithm, the total complexity can be expressed as

$$C_{\mathrm{TSS}} = \underbrace{2N_r}_{\text{Step1}} + \underbrace{2^{(R-\log_2 N_r)}[2N_r(N+T)(4N-1)+6N_r]}_{\text{Step2}}. \tag{11}$$

To illustrate the complexity comparison more intuitively, we present the exact flops of these two kinds of detectors under various parameter settings in Table I. Clearly, the implementation of the TSS detector exhibits a notably reduced computational complexity compared to the optimal ML detector. This reduction in complexity becomes more pronounced as N_r increases, benefiting from the reduced search space by separating the receive antenna index firstly.

III. PERFORMANCE ANALYSIS

A. ABER performance analysis

This subsection is dedicated to deriving a closed-form expression for the upper bound on the ABEP to perform theoretical analysis of the proposed scheme. By leveraging the widely recognized union bound technique, the ABEP of the proposed scheme is constrained by

$$\begin{aligned}\text{ABEP} \leq & \frac{1}{R2^R}\sum_i\sum_j\sum_k\sum_{\hat{i}}\sum_{\hat{j}}\sum_{\hat{k}} d\{(i,j,k)\to(\hat{i},\hat{j},\hat{k})\} \\ & \times \mathbb{P}\{(i,j,k)\to(\hat{i},\hat{j},\hat{k})\},\end{aligned} \tag{12}$$

where R is the transmission rate given in (29), $d\{(i,j,k)\to(\hat{i},\hat{j},\hat{k})\}$ is the Hamming distance and $\mathbb{P}\{(i,j,k)\to(\hat{i},\hat{j},\hat{k})\}$ denotes the UPEP.

For the sake of brevity, we use $\mathbb{P}_e$ and $\bar{\mathbb{P}}_e$ to denote CPEP and UPEP in the following text, respectively. To obtain the upper bound, we first derive the union upper bound of CPEP expression based on ML detection. Then, the closed-form expressions for the UPEP are obtained via PDF method.

- CPEP Analysis: The CPEP $\mathbb{P}_e$ of the proposed FA-JTR-IM system can be written as

$$\begin{aligned}\mathbb{P}_e &= \mathbb{P}\{(i,j,k)\to(\hat{i},\hat{j},\hat{k})\,|\mathbf{H},\mathbf{G}\} \\ &= \mathbb{P}\left\{\left\|\mathbf{y}-\sqrt{\frac{P}{N}}\mathbf{G}\mathrm{diag}(\mathbf{\Psi}_{ij})\mathbf{H}\mathbf{e}_j s_k\right\|_2^2\right. \\ &\qquad \left. > \left\|\mathbf{y}-\sqrt{\frac{P}{N}}\mathbf{G}\mathrm{diag}(\mathbf{\Psi}_{\hat{i}\hat{j}})\mathbf{H}\mathbf{e}_{\hat{j}} s_{\hat{k}}\right\|_2^2\right\}.\end{aligned} \tag{13}$$

According to the correctly detected and erroneously detected transmit FA position index and receive UPA element index, the derivation process can be divided into two categories: $(i,j)=(\hat{i},\hat{j})$ and $(i,j)\neq(\hat{i},\hat{j})$, which will be detailed as follows:

1) $(i,j)=(\hat{i},\hat{j})$: In this case, the detection of transmit FA position index and receive UPA element index are both correct, the error arises from the transmitted signal, i.e., $s_k \neq s_{\hat{k}}$. As a result, the CPEP in (13) can be further simplified as

$$\begin{aligned}\mathbb{P}_e =& \mathbb{P}\left\{2\Re\left\{\sqrt{P/N}\mathbf{w}^H\left(\mathbf{G}\mathrm{diag}(\mathbf{\Psi}_{ij})\mathbf{H}\mathbf{e}_j(s_k-s_{\hat{k}})\right)\right\}\right. \\ & \left. + \left\|\sqrt{P/N}\mathbf{G}\mathrm{diag}(\mathbf{\Psi}_{ij})\mathbf{H}\mathbf{e}_j(s_k-s_{\hat{k}})\right\|_2^2 < 0\right\}.\end{aligned} \tag{14}$$

Let $\zeta = 2\Re\{\sqrt{P/N}\mathbf{w}^H\Delta\} + \left\|\sqrt{P/N}\Delta\right\|_2^2$ for ease of notation, where $\Delta = \mathbf{G}\mathrm{diag}(\mathbf{\Psi}_{ij})\mathbf{H}\mathbf{e}_j(s_k-s_{\hat{k}})$. Since the elements of $\mathbf{w}^H$ has complex normal distribution with variance N_0, its real part has norm distribution with variance $\frac{N_0}{2}$, i.e., $\Re\{\mathbf{w}^H\}\sim\mathcal{CN}\left(0,\frac{N_0\mathbf{I}_{N_r}}{2}\right)$. Therefore, the random variable ζ follows $\mathcal{N}(\mu_\zeta,\sigma_\zeta^2)$, wherein $\mu_\zeta=\sqrt{P/N}\,\|\Delta\|_2^2$ and

$$\begin{aligned}\sigma_\zeta^2 &= \mathbb{E}\left[(\zeta-\mu_\zeta)^2\right] \\ &= \mathbb{E}\left[\left(2\Re\left\{\sqrt{P/N}\mathbf{w}^H\Delta\right\}\right)^2\right] \\ &= 4\sqrt{\frac{P}{N}}\mathbb{E}\left[\Re\{(\mathbf{w}^H)^2\}\right]\mathbb{E}\left[\Re\left\{\|\Delta\|_2^2\right\}\right] \\ &= 2N_0\sqrt{\frac{P}{N}}\|\Delta\|_2^2.\end{aligned} \tag{15}$$

Subsequently, the CPEP can be calculated as

$$\begin{aligned}\mathbb{P}_e &= Q\left(\sqrt{\frac{\|\Delta\|_2^2}{2N_0}}\right) \\ &= Q\left(\sqrt{\frac{\|\mathbf{G}\mathrm{diag}(\mathbf{\Psi}_{ij})\mathbf{H}\mathbf{e}_j\|_2^2|s_k-s_{\hat{k}}|^2}{2N_0}}\right).\end{aligned} \tag{16}$$

2) $(i,j)\neq(\hat{i},\hat{j})$: This case means that the detection of spatial symbol indices are wrong, which includes three cases as $(i=\hat{i},j\neq\hat{j})$, $(i\neq\hat{i},j=\hat{j})$ and $(i\neq\hat{i},j\neq\hat{j})$. Thus, the CPEP is written as

$$\mathbb{P}_e = \mathbb{P}\left\{\left\|\mathbf{w}^H\right\|_2^2 - \left\|\mathbf{w}^H+\sqrt{\frac{P}{N}}\Delta_{\mathbf{x}}\right\|_2^2 > 0\right\}, \tag{17}$$

where $\Delta_{\mathbf{x}} = \mathbf{G}\mathrm{diag}(\mathbf{\Psi}_{ij})\mathbf{H}\mathbf{e}_j s_k - \mathbf{G}\mathrm{diag}(\mathbf{\Psi}_{\hat{i}\hat{j}})\mathbf{H}\mathbf{e}_{\hat{j}} s_{\hat{k}}$. To simplify notation, we define two random variables χ_1 and χ_2

This article has been accepted for publication in IEEE Transactions on Wireless Communications. This is the author's version which has not been fully edited and content may change prior to final publication. Citation information: DOI 10.1109/TWC.2024.3511579

as

$$\chi_1 = \frac{\left\|\mathbf{w}^H\right\|_2^2}{N_0/2}, \tag{18}$$

and

$$\chi_2 = \frac{\left\|\mathbf{w}^H + \sqrt{\frac{P}{N}}\Delta_{\mathbf{x}}\right\|_2^2}{N_0/2}, \tag{19}$$

which are central and non-central Chi-square random variables with two degrees of freedom, respectively. The non-centrality parameter of χ_2 is

$$\Pi = \frac{2P\left\|\Delta_{\mathbf{x}}\right\|_2^2}{NN_0}. \tag{20}$$

Accordingly, the CPEP in (17) can be calculated as

$$\begin{aligned}\mathbb{P}_e &= \mathbb{P}(\chi_1 > \chi_2) \\ &= \int_0^\infty \int_{x_2}^\infty f_{\chi_1}(x_1) f_{\chi_2}(x_2)\mathrm{d}x_1\mathrm{d}x_2,\end{aligned} \tag{21}$$

where $f_{\chi_1}(x_1) = \frac{1}{2}\exp\left(-\frac{x_1}{2}\right)$ is the PDF of the central Chi-square random variable χ_1 and $f_{\chi_2}(x_2) = \frac{1}{2}\exp\left(-\frac{x_2+\Pi}{2}\right)\sum\limits_{i=0}^{\infty}\frac{\left(\frac{\Pi x_2}{4}\right)^i}{(i!)^2}$ is the PDF of the non-central Chi-square random variable χ_2.

Substituting the PDF of $f_{\chi_1}(x_1)$ and $f_{\chi_2}(x_2)$ into (21),

$$\begin{aligned}\mathbb{P}_e &= \frac{1}{4}\int\limits_0^\infty \exp\left(\frac{-(x_2+\Pi)}{2}\right) \\ &\quad \times \sum_{i=0}^{\infty}\frac{\left(\frac{\Pi x_2}{4}\right)^i}{(i!)^2}\left\{\int\limits_{x_2}^{\infty}\exp\left(\frac{-x_1}{2}\right)\mathrm{d}x_1\right\}\mathrm{d}x_2 \\ &= \frac{1}{2}\exp\left(-\frac{\Pi}{2}\right)\sum_{i=0}^{\infty}\left\{\frac{\left(\frac{\Pi}{4}\right)^i}{(i!)^2}\int\limits_0^\infty x_2^i\exp(-x_2)\mathrm{d}x_2\right\} \\ &\overset{(a)}{=} \frac{1}{2}\exp\left(-\frac{\Pi}{2}\right)\sum_{i=0}^{\infty}\frac{\left(\frac{\Pi}{4}\right)^i}{i!} \\ &\overset{(b)}{=} \frac{1}{2}\exp\left(-\frac{\Pi}{4}\right),\end{aligned} \tag{22}$$

where step (a) in (22) is obtained by using the integral that $\int_0^\infty x^i\exp(-x)\mathrm{d}x = i!$, while step (b) is derived by utilizing $\sum_{i=0}^{\infty}\frac{x^i}{i!} = \exp(x)$. Thus, the CPEP can be recast as

$$\mathbb{P}_e = \frac{1}{2}\exp\left(\frac{-P\left\|\mathbf{G}\mathrm{diag}(\mathbf{\Psi}_{ij})\mathbf{He}_j s_k - \mathbf{G}\mathrm{diag}(\mathbf{\Psi}_{\hat{i}\hat{j}})\mathbf{He}_{\hat{j}} s_{\hat{k}}\right\|_2^2}{2NN_0}\right). \tag{23}$$

- UPEP Analysis: We embark on the derivation of the UPEP utilizing the PDF method.

1) $(i,j) = (\hat{i},\hat{j})$: In this case, based on the CPEP derived in (16), the UPEP $\bar{\mathbb{P}}_e$ can be calculated by

$$\bar{\mathbb{P}}_e = \int\limits_0^\infty f(z_1)\, Q\left(\sqrt{\frac{z_1}{2N_0}}\right)\mathrm{d}z_1, \tag{24}$$

where $z_1 = \|\mathbf{G}\mathrm{diag}(\mathbf{\Psi}_{ij})\mathbf{He}_j\|_2^2\left|s_k - s_{\hat{k}}\right|^2$ and $f(z_1)$ is the PDF of z_1.

Lemma 1 *In the case of* $(i,j) = (\hat{i},\hat{j})$*, the analytical expression of UPEP can be expressed as*

$$\begin{aligned}\bar{\mathbb{P}}_e = &\frac{1}{2^{L+1}[(L-1)!]^2}\left(\frac{L}{c\mathbb{E}[B])}\right)^{L-1}\times \\ &\left[1-\omega(a)\sum_{k=0}^{L-1}\left(\begin{array}{c}2k\\k\end{array}\right)\left(\frac{1-\omega^2(a)}{4}\right)^k\right].\end{aligned} \tag{25}$$

where $B = |s_k - s_{\hat{k}}|^2\|\tilde{\mathbf{G}}\mathrm{diag}(\mathbf{\Psi}_{ij})\mathbf{h}(\mathbf{t}_{m,n})\|_2^2$, $\tilde{\mathbf{G}} = [\tilde{\mathbf{g}}(\mathbf{r}_{1,1}),...,\tilde{\mathbf{g}}(\mathbf{r}_{R_1,R_2})]^T$, and $\tilde{\mathbf{g}}(\mathbf{r}_{p,q}) = \mathbf{F}^H\mathbf{k}(\mathbf{r}_{p,q})$. $\omega(a) = \sqrt{\frac{a}{1+a}}$ with $a = \frac{|s_k - s_{\hat{k}}|^2}{4N_0}$, and

$$\mathbb{E}[B] = \begin{cases} N|s_k - s_{\hat{k}}|^2\mathbb{E}[\|\tilde{\mathbf{G}}\|_2^2], & \text{for } L \text{ is finite} \\ N|s_k - s_{\hat{k}}|^2\mathbf{R}, & \text{for } L \to \infty \end{cases}$$

with $\mathbf{R}$ *is the spatial correlation matrix of* $\tilde{\mathbf{G}}$.

Proof: See Appendix A.

2) $(i,j) \neq (\hat{i},\hat{j})$: In this case, the UPEP can be written as

$$\bar{\mathbb{P}}_e = \frac{1}{2}\int\limits_0^\infty f(z_2)\exp\left(-\frac{P}{2NN_0}z_2\right)\mathrm{d}z_2, \tag{26}$$

where $z_2 = \left\|\mathbf{G}\mathrm{diag}(\mathbf{\Psi}_{ij})\mathbf{He}_j s_k - \mathbf{G}\mathrm{diag}(\mathbf{\Psi}_{\hat{i}\hat{j}})\mathbf{He}_{\hat{j}} s_{\hat{k}}\right\|_2^2$.

Lemma 2 *In the case of* $(i,j) \neq (\hat{i},\hat{j})$*, the analytical expression of UPEP can be expressed as*

$$\bar{\mathbb{P}}_e = \frac{1}{2^{L+1}[(L-1)!]^2}\left(\frac{L}{c\mathbb{E}[\tilde{B}]}\right)^{L-1}\left(\frac{2LNN_0 + cP\mathbb{E}[\tilde{B}]}{2c\mathbb{E}[\tilde{B}]NN_0}\right)^L, \tag{27}$$

where $\tilde{B} = \left\|\tilde{\mathbf{G}}\left(\mathrm{diag}(\mathbf{\Psi}_{ij})\mathbf{He}_j s_k - \mathrm{diag}(\mathbf{\Psi}_{\hat{i}\hat{j}})\mathbf{He}_{\hat{j}} s_{\hat{k}}\right)\right\|_2^2$ *and*

$$\mathbb{E}[\tilde{B}] = \begin{cases} 2(N - \Re\{\Upsilon\})\mathbb{E}[\|\tilde{\mathbf{G}}\|_2^2], & \text{for } L \text{ is finite} \\ 2(N - \Re\{\Upsilon\})\mathbf{R}, & \text{for } L \to \infty \end{cases}$$

with $\Upsilon = s_k(s_{\hat{k}})^H\mathrm{diag}(\mathbf{\Psi}_{ij})(\mathrm{diag}(\mathbf{\Psi}_{\hat{i}\hat{j}}))^H\mathbf{He}_j(\mathbf{He}_{\hat{j}})^H$.

Proof: See Appendix B.

Remark 1: We observe from (25) and (27) that the UPEP $\bar{\mathbb{P}}_e$ is inversely proportional to $\mathbb{E}[\tilde{B}]$. Therefore, increasing N (which increases $\mathbb{E}[\tilde{B}]$) will decrease $\bar{\mathbb{P}}_e$. In other words, the number of RIS elements N directly impacts system performance by increasing expected value $\mathbb{E}[\tilde{B}]$, thereby leading to a decrease in the upper bound on ABEP.

B. Spectral efficiency analysis

This subsection analyzes the bits per channel use (bpcu) throughput of the proposed FA-JTR-IM scheme, where the FPA-assisted IM (FPA-IM) serves as its benchmark to demonstrate the superiority of the proposed scheme.

The SE of the classic FPA-IM scheme is given by

$$R_{\mathrm{FPA-IM}} = \log_2(N_r) + \log_2(M). \tag{28}$$

This article has been accepted for publication in IEEE Transactions on Wireless Communications. This is the author's version which has not been fully edited and content may change prior to final publication. Citation information: DOI 10.1109/TWC.2024.3511579

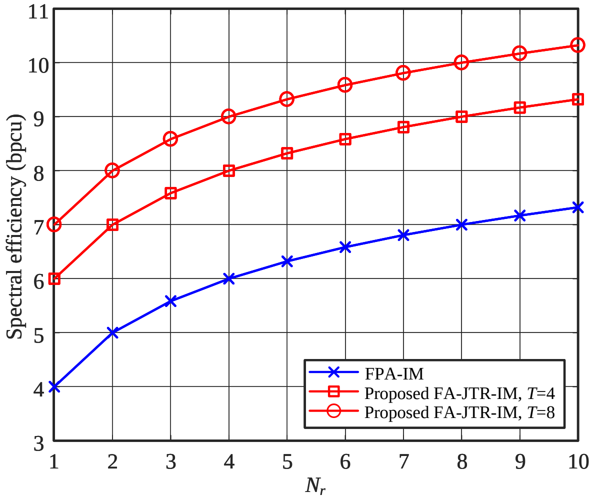

Fig. 2. Spectral efficiency comparisons between the proposed FA-JTR-IM with the conventional FPA-IM schemes.

Based on the signal model described in Section II-B, the SE of the proposed FA-JTR-IM scheme can be computed as

$$R_{\mathrm{FA-JTR-IM}} = \log_2(T) + \log_2(N_r) + \log_2(M). \tag{29}$$

To illustrate the SE performance more intuitively, Fig. 2 compares the SE between the proposed FA-JTR-IM and the conventional FPA-IM scheme for various numbers of receive antennas. The results show that the proposed scheme offers a significant SE increase compared to the conventional FPA-IM scheme when a single antenna is equipped at the transmitter. This improvement is achieved by exploiting the spatial diversity provided by FA, as indicated by the first term, $\log_2(T)$, in (29)).

C. Implementation challenges of the proposed FA-JTR-IM system

In this subsection, we discuss several practical challenges associated with implementing the proposed system, including channel estimation and antenna movement.

1) Channel estimation: Channel estimation is a critical and challenging aspect of implementing FA-assisted systems. This issue has been extensively explored in various studies [10], [46], [47]. Specifically, the authors of [10] and [46] proposed a compressed sensing framework to leverage the inherent sparsity of the field-response-based channel model, enabling accurate channel reconstruction. Furthermore, a novel approach based on tensor decomposition for channel estimation and reconstruction for FA-enabled MIMO systems was introduced in [47], which is particularly effective for FA-enabled MIMO systems. These existing channel estimation algorithms are well-suited for the proposed FA-aided RIS system due to the similarity in the underlying channel models, where sparse and structured signals can be exploited for efficient channel estimation.

2) Antenna movement: Antenna movement can be achieved through various mechanical systems, microelectromechanical systems (MEMS) and reconfigurable pixel antennas, providing flexibility to meet the diverse requirements of wireless communication systems [7], [48], [49]. A common approach involves using stepper motors to mechanically adjust the antenna's position via drive components [7]. These motors provide precise control, making them ideal for larger systems where scalability is important. However, FAs that rely on mechanical movement face significant challenges in high-mobility scenarios due to the time required for antenna repositioning. This delay hampers their ability to adapt to rapidly changing channel conditions, presenting a major obstacle in high-mobility communications.

TABLE II
SIMULATION PARAMETERS.

Parameter	**Assumed value**
Carrier frequency f	28 GHz
Wavelength λ	0.01 m
Distance from RIS to Rx d	30 m
Unit distance path loss c_0	-62 dB
Path loss exponent ϖ	2.8
Transmit/receive region	$10\lambda \times 10\lambda$

Alternatively, MEMS-integrated antennas [48] and reconfigurable pixel antennas [49] provide a more compact and efficient solution, particularly for small-scale systems such as mmWave and terahertz (THz) transceivers. These technologies offer high positioning accuracy, low power consumption, and miniaturized components, making them ideal for space-constrained devices. The precise control and high linearity provided by MEMS and reconfigurable pixel antenna technologies further enhance antenna movement, making them highly suitable for the proposed FA-JTR-IM scheme.

IV. SIMULATION RESULTS

This section showcases simulation results aimed at evaluating the effectiveness of the proposed FA-JTR-IM scheme and confirming the accuracy of the analytical upper bound derived for ABEP. The simulation parameters are given in Table II. In this work, we assume that the noise power spectral density (PSD) is -174 dBm/Hz [50]. Given a bandwidth (BW) of 100 MHz, the noise power can be calculated as $N_0 = \mathrm{PSD} + 10\log_{10}(BW) = -94$ dBm. For all simulation results, we set the transmit power to range from 10 dBm to 40 dBm, which corresponds to an SNR range of 1 dB to 31 dB.

The performance of the proposed FA-JTR-IM scheme is illustrated in Figs. 3 and 4 through both simulated and analytical average BER results. More precisely, Fig. 3 shows the error performance over the finite-path channel condition (i.e., $L = 10$), while Fig. 4 is depicts the performance under the infinite-path channel condition (i.e., $L = 100$). As shown in Fig. 3, in the finite-path case, as the transmission rate increases, there is a notable increase in the disparity between the simulated outcomes and the theoretical upper bound. This divergences is rooted in the inherent characteristics of the upper bound, which essentially provides an approximation and is thus subject to constraints that become more pronounced

This article has been accepted for publication in IEEE Transactions on Wireless Communications. This is the author's version which has not been fully edited and content may change prior to final publication. Citation information: DOI 10.1109/TWC.2024.3511579

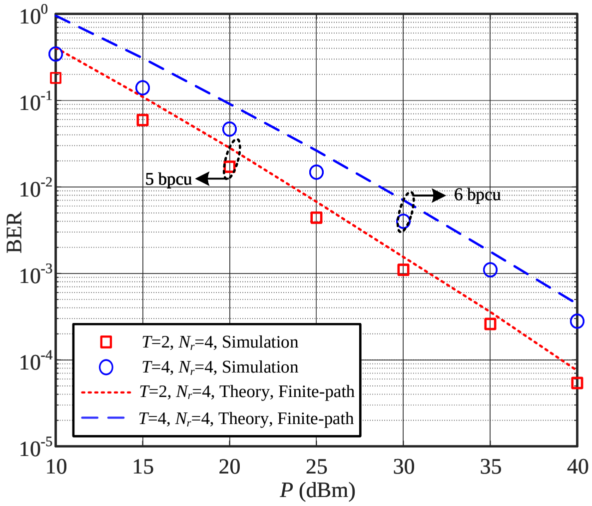

Fig. 3. Simulation and theoretical results of the proposed FA-JTR-IM scheme using the optimal ML detector under various parameter setting with $N = 16$, $L = 10$, and 4QAM modulation.

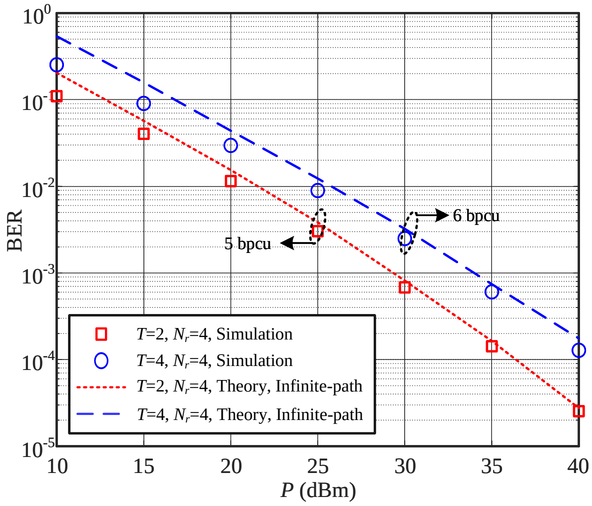

Fig. 4. Simulation and theoretical results of the proposed FA-JTR-IM scheme using the optimal ML detector under various parameter setting with $N = 16$, $L = 100$, and 4QAM modulation.

as transmission rate escalates. However, in the infinite-path case as shown in Fig. 4, the theoretical upper bound evinces a propensity to converge more closely towards the simulated results, especially in the high transmit power P region. In the case of infinite-path channel, we provide a closed-form expression for the UPEP. This provision stands as a pivotal contribution, furnishing an invaluable theoretical tool for the comprehensive evaluation of the system performance.

Fig. 5 compares the BER performance of the proposed FA-JTR-IM scheme at data rate of 6 bpcu under $T = 4$, $N_r = 4$, $L = 10$, 4QAM and various number of RIS elements N. It can be observed from Fig. 5 that the proposed FA-JTR-IM framework with increasing N achieves a significant enhancement in BER performance. This enhancement is principally attributable to the increased number of RIS elements, improving the SNR of the received signal. Furthermore, Fig. 6 presents BER comparisons of the proposed FA-JTR-IM scheme employing BPSK, 4QAM and 16QAM constellations at transmission rates of 5 bpcu, 6 bpcu and 8 bpcu, respectively. Evidently, when the target BER is 10^{-3}, systems with 4QAM and 16QAM require approximately 3 dBm and 8 dBm higher transmit power, respectively, compared to the BPSK system. This phenomenon is due to the fact that the increase in modulation order leads to a denser distribution of constellation points within the normalized symbol constellation diagram, consequently resulting in diminished Euclidean distances between adjacent constellation points.

Fig. 7 compares the error performance of the proposed FA-JTR-IM scheme with its benchmark systems under the same transmission rate condition, where “FA-T-IM” refers to the FA-aided transmit IM scheme, “RSM” refers to the receive IM scheme, and “SIMO without IM” denotes the conventional FPAs-assisted SIMO scheme without IM. In the case of $N_t = 1$, $N_r = 4$, $N = 128$ and $L = 10$, we set the simulation parameters as $T = 4$ and 4QAM in the proposed FA-JTR-IM scheme, $T = 4$ and 16QAM in the FA-T-IM scheme, 16QAM in the RSM scheme, and 64QAM in the SIMO without IM scheme, to achieve the transmission rate of 6 bpcu. It can be seen from Fig. 7 that the proposed FA-JTR-IM significantly outperforms the benchmark schemes in the high transmit power region. To be specific, at BER $= 10^{-3}$, the proposed scheme offers 5 dB, 7.5 dB and over 10 dB transmit power gains compared to the FA-T-IM, RSM and SIMO without IM schemes, respectively. This is primarily due to the fact that, in the high transmit power region, symbol detection errors become predominant, whereas in the low transmit power region, errors in estimating index symbol dominate.

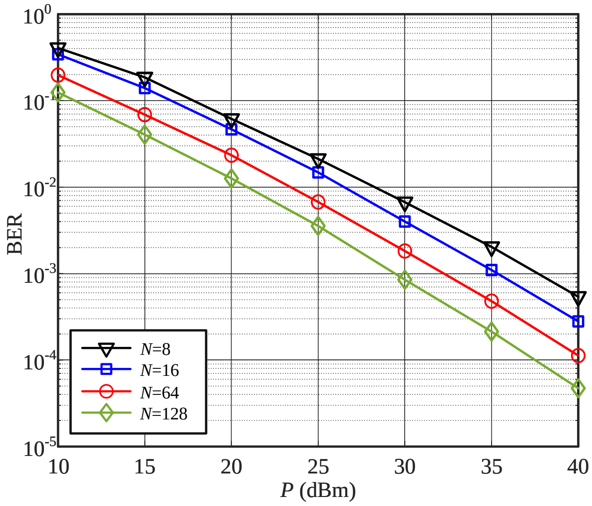

Fig. 5. BER performance of the proposed FA-JTR-IM scheme with $T = 4$, $N_r = 4$, $L = 10$ and 4QAM and various N.

Fig. 8 compares the detection performance of the optimal ML detector and the proposed TSS detector. As expected, the optimal ML detector exhibits superior error performance over the TSS detector. Specifically, in the case of 6 bpcu with $T = 4$, $N_r = 4$, $N = 128$ and 4QAM, the optimal ML detector provides a transmit power gain of 2.5 dB compared to the TSS detector when BER $= 10^{-3}$, but with 75% increase in computational complexity. It can be also observed from

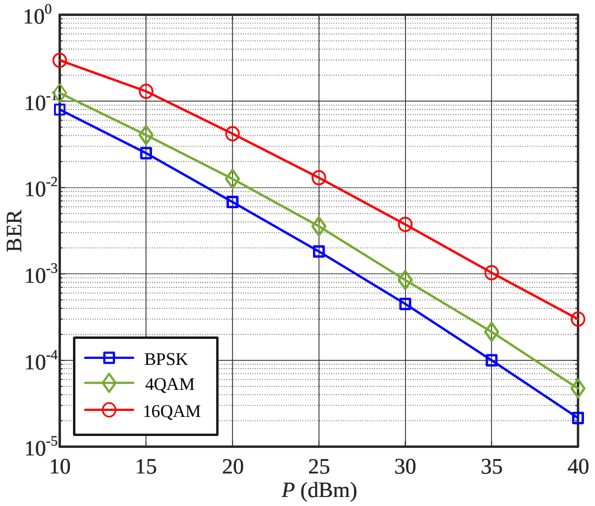

Fig. 6. BER performance of the proposed FA-JTR-IM scheme for the simulation parameters with $T = 4$, $N_r = 4$, $L = 10$ and $N = 128$ and various modulation order M.

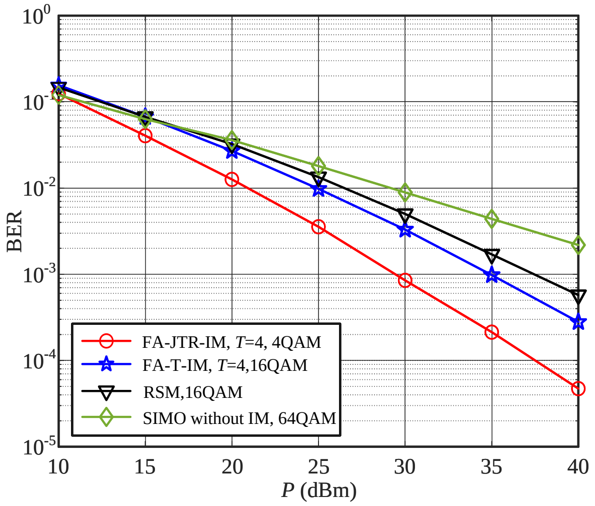

Fig. 7. BER performance comparisons between the proposed FA-JTR-IM scheme and its benchmark schemes at transmission rate of 6 bpcu.

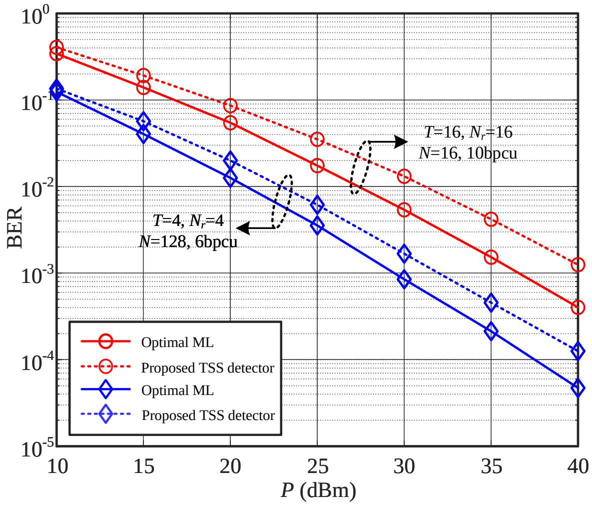

Fig. 8. BER performance comparison of the optimal ML and proposed TSS detectors for the proposed FA-JTR-IM scheme.

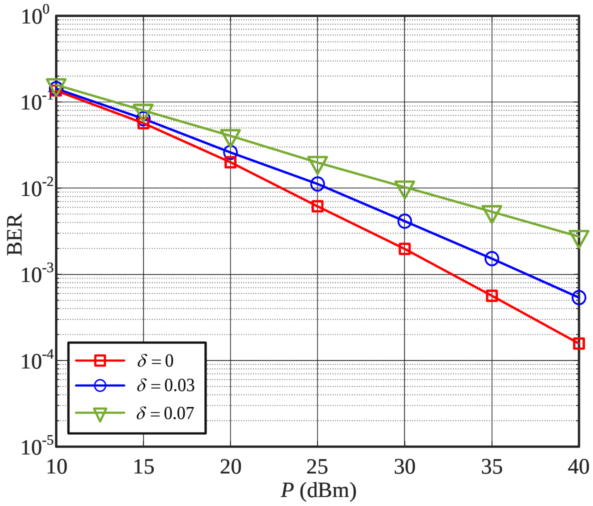

Fig. 9. BER performance at 6 bpcu ($T = 4$, $N_r = 4$, $N = 16$, $L = 10$ and 4QAM) for the TSS detector aided FA-JTR-IM schemes in perfect and imperfect CSI cases.

Fig. 8 that the detection performance gap between these two detectors becomes larger as the number of receive antennas N_r increases. Correspondingly, as shown in Table I, the reduction in detection complexity becomes more significant. This is because that the increase in receive antennas means an increase in the receive index bits, however, the first step of the TSS detector is to estimate the receive index bits, which will degrade the overall error performance.

Fig. 9 evaluates the impact of channel estimation errors on the BER performance of the TSS detector in the proposed FA-JTR-IM scheme. Here, the imperfect channel matrices are modeled as $\mathbf{H}_e = \mathbf{H} + \mathbf{H}_\mathrm{t}$ and $\mathbf{G}_e = \mathbf{G} + \mathbf{H}_\mathrm{r}$, where $\mathbf{H}_\mathrm{t}$ and $\mathbf{H}_\mathrm{r}$ are the channel error with its entries being $\mathcal{CN}(0, \delta^2)$ [51]. It is worth mentioning that the performance of the perfect CSI case (i.e., $\delta = 0$) is also included to facilitate comparative analysis. It can be seen from Fig. 9 that the error performance of the TSS detector deteriorates with an increase in δ. Specifically, when BER is 10^{-2}, the transmit power deterioration of the TSS detector is 2 dB and 7 dB for $\delta = 0.03$ and $\delta = 0.07$, respectively, compared to the perfect CSI case. These results demonstrate that the proposed FA-JTR-IM scheme is sensitive to CSI errors, as the BER performance degrades noticeably with increasing δ, indicating that precise CSI estimation is crucial for maintaining optimal performance.

V. CONCLUSION

In this paper, we proposed a novel FA empowered joint transmit and receive IM transmission scheme for RIS-assisted mmWave SIMO communication systems, which can significantly enhance the SE while retaining a single-RF transceiver structure by the integration of RIS, FA and IM techniques. In addition, we explored two detection algorithms, maximizing detection accuracy with ML detector while offering computational efficiency through the TSS algorithm. Furthermore, the analysis of the ABEP was conducted, and simulation

This article has been accepted for publication in IEEE Transactions on Wireless Communications. This is the author's version which has not been fully edited and content may change prior to final publication. Citation information: DOI 10.1109/TWC.2024.3511579

results confirmed the accuracy of the theoretical analysis, demonstrating the advantage of the proposed FA-JTR-IM scheme over its benchmarks. Overall, the proposed FA-JTR-IM scheme constitutes a promising candidate solution for RIS-assisted mmWave communications.

APPENDIX A
PROOF OF LEMMA 1

According to (1), (2) and (3), the random variable z_1 can be written as

$$\begin{aligned} z_1 &= \left|s_k - s_{\hat{k}}\right|^2 \|\mathbf{G}\mathrm{diag}(\mathbf{\Psi}_{ij})\mathbf{H}\mathbf{e}_j\|_2^2 \\ &= \left|s_k - s_{\hat{k}}\right|^2 \|\tilde{\mathbf{G}}\mathrm{diag}(\mathbf{\Psi}_{ij})\mathbf{h}(\mathbf{t}_{m,n})\|_2^2 \, \|\mathbf{\Xi}\|_2^2 , \end{aligned} \tag{30}$$

where $\tilde{\mathbf{G}} = [\tilde{\mathbf{g}}(\mathbf{r}_{1,1}), ..., \tilde{\mathbf{g}}(\mathbf{r}_{p,q}), ..., \tilde{\mathbf{g}}(\mathbf{r}_{R_1,R_2})]^T \in \mathbb{C}^{N_r \times N}$ and $\tilde{\mathbf{g}}(\mathbf{r}_{p,q}) = \mathbf{F}^H\mathbf{k}(\mathbf{r}_{p,q}) \in \mathbb{C}^{N\times 1}$. Since $\mathbf{\Xi}$ is the PRM, whose elements obey $\mathcal{CN}(0, c/L)$, z_1 follows the generalized central Chi-square distribution with $2L$ degree of freedom. The PDF of z_1 is given by

$$f(z_1) = \frac{1}{2^L(L-1)!}\left(\frac{Lz_1}{cB}\right)^{L-1} \exp\left(-\frac{Lz_1}{cB}\right), \tag{31}$$

where $B = |s_k - s_{\hat{k}}|^2 \|\tilde{\mathbf{G}}\mathrm{diag}(\mathbf{\Psi}_{ij})\mathbf{h}(\mathbf{t}_{m,n})\|_2^2$.

Substituting (47) into (24), the UPEP can be calculated as

$$\begin{aligned} \bar{\mathbb{P}}_e = \frac{1}{\pi 2^L(L-1)!} \int_0^{\infty}\int_0^{\pi/2} \left(\frac{Lz_1}{cB}\right)^{L-1} \exp\left(-\frac{Lz_1}{cB}\right) \\ \times \exp\left(-\frac{z_1}{4N_0 \sin^2\theta}\right) \mathrm{d}\theta \mathrm{d}z_1. \end{aligned} \tag{32}$$

By exchanging the order of integration, (32) can be further expressed as

$$\begin{aligned} \bar{\mathbb{P}}_e &= \frac{1}{\pi 2^L(L-1)!} \int_0^{\pi/2}\int_0^{\infty} \left(\frac{Lz_1}{cB}\right)^{L-1} \\ &\qquad \times \exp\left(-\frac{4LN_0\sin^2\theta + cB}{4cBN_0\sin^2\theta} z\right) \mathrm{d}z_1 \mathrm{d}\theta \\ &= \frac{1}{\pi 2^L[(L-1)!]^2}\left(\frac{L}{cB}\right)^{L-1} \int_0^{\pi/2} \left(\frac{\sin^2\theta}{\sin^2\theta + \frac{|s_k - s_{\hat{k}}|^2}{4N_0}}\right)^L \mathrm{d}\theta. \end{aligned} \tag{33}$$

Based on the integral formula in [52]

$$\begin{aligned} &\frac{1}{\pi}\int_0^{\pi/2}\left(\frac{\sin^2\theta}{\sin^2\theta + a}\right)^L \mathrm{d}\theta \\ &\quad = \frac{1}{2}\left[1 - \omega(a)\sum_{k=0}^{L-1}\begin{pmatrix} 2k \\ k \end{pmatrix}\left(\frac{1-\omega^2(a)}{4}\right)^k\right], \end{aligned} \tag{34}$$

where $\omega(a) = \sqrt{\frac{a}{1+a}}$, the UPEP in (33) can be rewritten as

$$\begin{aligned} \bar{\mathbb{P}}_e =& \frac{1}{2^{L+1}[(L-1)!]^2}\left(\frac{L}{cB}\right)^{L-1} \times \\ &\left[1 - \omega(a)\sum_{k=0}^{L-1}\begin{pmatrix} 2k \\ k \end{pmatrix}\left(\frac{1-\omega^2(a)}{4}\right)^k\right], \end{aligned} \tag{35}$$

where $a = \frac{|s_k - s_{\hat{k}}|^2}{4N_0}$. Furthermore, the UPEP $\bar{\mathbb{P}}_e$ can be further obtained by taking expectation over the parameter B as

$$\begin{aligned} \bar{\mathbb{P}}_e = & \frac{1}{2^{L+1}[(L-1)!]^2}\left(\frac{L}{c\mathbb{E}[B])}\right)^{L-1} \times \\ & \left[1 - \omega(a)\sum_{k=0}^{L-1}\begin{pmatrix} 2k \\ k \end{pmatrix}\left(\frac{1-\omega^2(a)}{4}\right)^k\right]. \end{aligned} \tag{36}$$

Next, we will discuss the value of $\mathbb{E}[B]$ in two cases, i.e., finite-path (L is finite) case and infinite-path ($L \to \infty$) case.

- *Finite-path case*: In this case, acquiring the precise distribution of elements within $\tilde{\mathbf{G}}$ poses a challenge. However, the approximate $\mathbb{E}[\tilde{\mathbf{G}}]$ can be obtained by the Monte Carlo method, so the value of $\mathbb{E}[B]$ can thus be calculated by

$$\begin{aligned} \mathbb{E}[B] &= |s_k - s_{\hat{k}}|^2 \mathbb{E}[\|\tilde{\mathbf{G}}\mathrm{diag}(\mathbf{\Psi}_{ij})\mathbf{h}(\mathbf{t}_{m,n})\|_2^2] \\ &= |s_k - s_{\hat{k}}|^2 \mathbb{E}[\|\tilde{\mathbf{G}}\|_2^2]\mathbb{E}[\|\mathbf{h}(\mathbf{t}_{m,n})\|_2^2] \\ &= N|s_k - s_{\hat{k}}|^2 \mathbb{E}[\|\tilde{\mathbf{G}}\|_2^2]. \end{aligned} \tag{37}$$

- *Infinite-path case*: To begin, let's first revisit the expression of $\tilde{\mathbf{g}}(\mathbf{r}_{p,q})$, which is given by

$$\tilde{\mathbf{g}}(\mathbf{r}_{p,q}) = \mathbf{F}^H\mathbf{k}(\mathbf{r}_{p,q}) = \sum_{l=1}^{L} g_l \mathbf{a}(\theta_{\mathrm{R},l}, \phi_{\mathrm{R},l}), \tag{38}$$

where $g_l = e^{\jmath\frac{2\pi}{\lambda}\rho_{\mathrm{r},l}(\mathbf{r}_{p,q})}$ and $\mathbf{a}(\theta_{\mathrm{R},l}, \phi_{\mathrm{R},l})$ is the lth row of the FRM $\mathbf{F}$, denoted as

$$\mathbf{a}(\theta_{\mathrm{R},l}, \phi_{\mathrm{R},l}) = [\rho_{\mathrm{R},l}(\mathbf{n}_{1,1}), \rho_{\mathrm{R},l}(\mathbf{n}_{1,2}), ..., \rho_{\mathrm{R},l}(\mathbf{n}_{N_1,N_2})]^T. \tag{39}$$

As $L \to \infty$, the central limit theorem (CLT) dictates that

$$\tilde{\mathbf{g}}(\mathbf{r}_{p,q}) \sim \mathcal{N}(\mathbf{0}, \mathbf{R}), \tag{40}$$

where the calculation of the normalized spatial correlation matrix $\mathbf{R} \in \mathbb{C}^{N\times N}$ is performed as

$$\mathbf{R} = \mathbb{E}\{\tilde{\mathbf{g}}(\mathbf{r}_{p,q})\tilde{\mathbf{g}}(\mathbf{r}_{p,q})^H\} = \mathbb{E}\{\mathbf{a}(\theta_{\mathrm{r},l}, \phi_{\mathrm{r},l})\mathbf{a}(\theta_{\mathrm{r},l}, \phi_{\mathrm{r},l})^H\}. \tag{41}$$

Next, we will give the procedure for calculating $\mathbf{R}$. Specifically, the (i, j)th entry in $\mathbf{R}$ is expressed as

$$\begin{aligned} [\mathbf{R}]_{i,j} &= \mathbb{E}\{\mathbf{a}(\theta_{\mathrm{R},l}, \phi_{\mathrm{R},l})(i)\mathbf{a}(\theta_{\mathrm{R},l}, \phi_{\mathrm{R},l})(j)^H\} \\ &= \mathbb{E}\{e^{\jmath\frac{2\pi}{\lambda}((x_{\mathrm{R},u} - x_{\mathrm{R},p})\cos\theta_{\mathrm{R},l}\sin\phi_{\mathrm{R},l} + (y_{\mathrm{R},v} - y_{\mathrm{R},q})\sin\theta_{\mathrm{R},l})}\}, \end{aligned} \tag{42}$$

where $i, j \in \{1, 2, ..., N\}$ and satisfies the relationship with the pairs (u, v) and (p, q) as $i = (u-1)N_2 + v$ and $j = (p-1)N_2 + q$, $u, p \in \{1, 2, ..., N_1\}$ and $v, q \in \{1, 2, ..., N_2\}$.

Multi-path components in environments with isotropic scattering are evenly spread throughout the half-space in front of the UPA. This uniform distribution results in the AoAs following a PDF as

$$f(\theta_{\mathrm{R},l}, \phi_{\mathrm{R},l}) = \frac{\cos\theta_{\mathrm{R},l}}{2\pi}, \theta_{\mathrm{R},l} \in [-\frac{\pi}{2}, \frac{\pi}{2}], \phi_{\mathrm{R},l} \in [-\frac{\pi}{2}, \frac{\pi}{2}]. \tag{43}$$

This article has been accepted for publication in IEEE Transactions on Wireless Communications. This is the author's version which has not been fully edited and content may change prior to final publication. Citation information: DOI 10.1109/TWC.2024.3511579

Consequently, the expression in (42) can be further computed as

$$\begin{aligned}[\mathbf{R}]_{i,j} &= \int_{-\pi/2}^{\pi/2}\int_{-\pi/2}^{\pi/2} e^{\jmath\frac{2\pi}{\lambda}\|\mathbf{n}_{u,v}-\mathbf{n}_{p,q}\|\sin\theta_{\mathrm{R},l}} f(\theta_{\mathrm{R},l},\phi_{\mathrm{R},l})\mathrm{d}\theta_{\mathrm{R},l}\mathrm{d}\phi_{\mathrm{R},l} \\ &= \int_{-\pi/2}^{\pi/2} e^{\jmath\frac{2\pi}{\lambda}\|\mathbf{n}_{u,v}-\mathbf{n}_{p,q}\|\sin\theta_{\mathrm{R},l}} \frac{\cos\theta_{\mathrm{R},l}}{2\pi}\mathrm{d}\theta_{\mathrm{R},l} \\ &= \frac{\sin(\frac{2\pi}{\lambda}\left\|\mathbf{n}_{u,v}-\mathbf{n}_{p,q}\right\|)}{\frac{2\pi}{\lambda}\left\|\mathbf{n}_{u,v}-\mathbf{n}_{p,q}\right\|}.\end{aligned} \tag{44}$$

Since $\tilde{\mathbf{G}}$ is composed of multiple vectors $\tilde{\mathbf{g}}(\mathbf{r}_{p,q})$, each drawn independently from the same $\mathcal{N}(\mathbf{0},\mathbf{R})$ distribution. In such case, the distribution of the matrix $\tilde{\mathbf{G}}$ approximates $\mathcal{N}(\mathbf{0},\mathbf{R})$, therefore, (37) can be simplified as

$$\mathbb{E}[B] = N|s_k - s_{\hat{k}}|^2\mathbf{R}. \tag{45}$$

Combining (36), (37) and (45), the UPEP in the case of $(i,j) = (\hat{\imath},\hat{\jmath})$ can be summarised as **Lemma 1**.

APPENDIX B
PROOF OF LEMMA 2

In the case of $(i,j) \neq (\hat{\imath},\hat{\jmath})$, the random variable z_2 can be transformed as

$$\begin{aligned} z_2 &= \left\|\mathbf{G}\mathrm{diag}(\mathbf{\Psi}_{ij})\mathbf{H}\mathbf{e}_j s_k - \mathbf{G}\mathrm{diag}(\mathbf{\Psi}_{\hat{\imath}\hat{\jmath}})\mathbf{H}\mathbf{e}_{\hat{\jmath}} s_{\hat{k}}\right\|_2^2 \\ &= \left\|\tilde{\mathbf{G}}\left(\mathrm{diag}(\mathbf{\Psi}_{ij})\mathbf{H}\mathbf{e}_j s_k - \mathrm{diag}(\mathbf{\Psi}_{\hat{\imath}\hat{\jmath}})\mathbf{H}\mathbf{e}_{\hat{\jmath}} s_{\hat{k}}\right)\right\|_2^2 \|\mathbf{\Xi}\|_2^2 .\end{aligned} \tag{46}$$

Similar to the derivation process shown in Appendix A, the PDF of z_2 can be expressed as

$$f(z_2) = \frac{1}{2^L(L-1)!}\left(\frac{Lz_2}{c\tilde{B}}\right)^{L-1}\exp\left(-\frac{Lz_2}{c\tilde{B}}\right), \tag{47}$$

where $\tilde{B} = \left\|\tilde{\mathbf{G}}\left(\mathrm{diag}(\mathbf{\Psi}_{ij})\mathbf{H}\mathbf{e}_j s_k - \mathrm{diag}(\mathbf{\Psi}_{\hat{\imath}\hat{\jmath}})\mathbf{H}\mathbf{e}_{\hat{\jmath}} s_{\hat{k}}\right)\right\|_2^2$. Combining (26) and (47), the UPEP can be further calculated by

$$\begin{aligned}\bar{\mathbb{P}}_e &= \frac{1}{2^{L+1}(L-1)!}\int_0^\infty \left(\frac{Lz_2}{c\tilde{B}}\right)^{L-1}\times \\ &\qquad \exp\left(-\frac{Lz_2}{c\tilde{B}}\right)\exp\left(-\frac{P}{2NN_0}z_2\right)\mathrm{d}z_2 \\ &= \frac{1}{2^{L+1}(L-1)!}\int_0^\infty \left(\frac{Lz_2}{c\tilde{B}}\right)^{L-1}\exp\left(-\frac{2LNN_0+c\tilde{B}P}{2c\tilde{B}NN_0}z_2\right)\mathrm{d}z_2 \\ &= \frac{1}{2^{L+1}[(L-1)!]^2}\left(\frac{L}{c\tilde{B}}\right)^{L-1}\left(\frac{2LNN_0+c\tilde{B}P}{2c\tilde{B}NN_0}\right)^L .\end{aligned} \tag{48}$$

The same as the derivation process shown in Appendix A, the UPEP can further rewritten as

$$\bar{\mathbb{P}}_e = \frac{1}{2^{L+1}[(L-1)!]^2}\left(\frac{L}{c\mathbb{E}[\tilde{B}]}\right)^{L-1}\left(\frac{2LNN_0+cP\mathbb{E}[\tilde{B}]}{2c\mathbb{E}[\tilde{B}]NN_0}\right)^L , \tag{49}$$

where the calculation of $\mathbb{E}[\tilde{B}]$ is also divided into two cases as

- *finite-path case*: In this case, we have

$$\begin{aligned}\mathbb{E}[\tilde{B}] &= \mathbb{E}[|\tilde{\mathbf{G}}(\mathrm{diag}(\mathbf{\Psi}_{ij})\mathbf{H}\mathbf{e}_j s_k - \mathrm{diag}(\mathbf{\Psi}_{\hat{\imath}\hat{\jmath}})\mathbf{H}\mathbf{e}_{\hat{\jmath}} s_{\hat{k}})\|_2^2] \\ &= \mathbb{E}[|\tilde{\mathbf{G}}\|_2^2]\mathbb{E}[\|(\mathrm{diag}(\mathbf{\Psi}_{ij})\mathbf{H}\mathbf{e}_j s_k - \mathrm{diag}(\mathbf{\Psi}_{\hat{\imath}\hat{\jmath}})\mathbf{H}\mathbf{e}_{\hat{\jmath}} s_{\hat{k}})\|_2^2] \\ &= 2(N-\Re\{\Upsilon\})\mathbb{E}[\|\tilde{\mathbf{G}}\|_2^2],\end{aligned} \tag{50}$$

where $\Upsilon = s_k(s_{\hat{k}})^H\mathrm{diag}(\mathbf{\Psi}_{ij})(\mathrm{diag}(\mathbf{\Psi}_{\hat{\imath}\hat{\jmath}}))^H\mathbf{H}\mathbf{e}_j(\mathbf{H}\mathbf{e}_{\hat{\jmath}})^H$.

- *Infinite-path case*: In this case, $\mathbb{E}[\tilde{B}]$ is computed as

$$\mathbb{E}[\tilde{B}] = 2(N-\Re\{\Upsilon\})\mathbf{R}. \tag{51}$$

To integrate (49), (50) and (51), the UPEP in the case of $(i,j) \neq (\hat{\imath},\hat{\jmath})$ can be represented as **Lemma 2**.

REFERENCES

[1] S. Ju, Y. Xing, O. Kanhere, and T. S. Rappaport, "Millimeter wave and sub-terahertz spatial statistical channel model for an indoor office building," *IEEE J. Sel. Areas Commun.*, vol. 39, no. 6, pp. 1561–1575, Jun. 2021.

[2] M. R. Akdeniz, Y. Liu, M. K. Samimi, S. Sun, S. Rangan, T. S. Rappaport, and E. Erkip, "Millimeter wave channel modeling and cellular capacity evaluation," *IEEE J. Sel. Areas Commun.*, vol. 32, no. 6, pp. 1164–1179, Jun. 2014.

[3] S. A. Busari, K. M. S. Huq, S. Mumtaz, L. Dai, and J. Rodriguez, "Millimeter-wave massive MIMO communication for future wireless systems: A survey," *IEEE Commun. Surveys Tuts.*, vol. 20, no. 2, pp. 836–869, 2nd Quart. 2018.

[4] L. Zhu and K.-K. Wong, "Historical review of fluid antenna and movable antenna," *arXiv preprint arXiv:2401.02362*, 2024.

[5] K.-K. Wong, A. Shojaeifard, K.-F. Tong, and Y. Zhang, "Fluid antenna systems," *IEEE Trans. Wireless Commun.*, vol. 20, no. 3, pp. 1950–1962, Mar. 2021.

[6] K.-K. Wong, K.-F. Tong, Y. Shen, Y. Chen, and Y. Zhang, "Bruce Lee-inspired fluid antenna system: Six research topics and the potentials for 6G," *Frontiers Commun. Netw.*, vol. 3, p. 853416, Mar. 2022.

[7] L. Zhu, W. Ma, and R. Zhang, "Movable antennas for wireless communication: Opportunities and challenges," *IEEE Commun. Mag.*, 2023, early access, DOI: 10.1109/MCOM.001.2300212.

[8] L. Zhu, W. Ma, and R. Zhang, "Modeling and performance analysis for movable antenna enabled wireless communications," *IEEE Trans. Wireless Commun.*, 2023, early access, DOI: 10.1109/TWC.2023.3330887.

[9] C. Skouroumounis and I. Krikidis, "Fluid antenna with linear MMSE channel estimation for large-scale cellular networks," *IEEE Trans. Commun.*, vol. 71, no. 2, pp. 1112–1125, Feb. 2023.

[10] W. Ma, L. Zhu, and R. Zhang, "Compressed sensing based channel estimation for movable antenna communications," *IEEE Commun. Lett.*, vol. 27, no. 10, pp. 2747–2751, Oct. 2023.

[11] Z. Chai, K.-K. Wong, K.-F. Tong, Y. Chen, and Y. Zhang, "Port selection for fluid antenna systems," *IEEE Commun. Lett.*, vol. 26, no. 5, pp. 1180–1184, May 2022.

[12] W. Ma, L. Zhu, and R. Zhang, "MIMO capacity characterization for movable antenna systems," *IEEE Trans. Wireless Commun.*, 2023, early access, DOI: 10.1109/TWC.2023.3307696.

[13] J. D. Vega-Sánchez, L. Urquiza-Aguiar, H. R. C. Mora, N. V. O. Garzón, and D. P. M. Osorio, "Fluid antenna system: Secrecy outage probability analysis," *IEEE Trans. Veh. Technol.*, 2024, early access, DOI: 10.1109/TVT.2024.3376475.

[14] W. K. New, K.-K. Wong, H. Xu, K.-F. Tong, and C.-B. Chae, "Fluid antenna system: New insights on outage probability and diversity gain," *IEEE Trans. Wireless Commun.*, vol. 23, no. 1, pp. 128–140, Jan. 2024.

[15] C. Psomas, G. M. Kraidy, K.-K. Wong, and I. Krikidis, "On the diversity and coded modulation design of fluid antenna systems," *IEEE Trans. Wireless Commun.*, vol. 23, no. 3, pp. 2082–2096, Mar. 2024.

[16] L. Zhu, W. Ma, and R. Zhang, "Movable-antenna array enhanced beamforming: Achieving full array gain with null steering," *IEEE Commun. Lett.*, vol. 27, no. 12, pp. 3340–3344, Dec. 2023.

[17] W. Ma, L. Zhu, and R. Zhang, "Multi-beam forming with movable-antenna array," *IEEE Commun. Lett.*, vol. 28, no. 3, pp. 697–701, Mar. 2024.

This article has been accepted for publication in IEEE Transactions on Wireless Communications. This is the author's version which has not been fully edited and content may change prior to final publication. Citation information: DOI 10.1109/TWC.2024.3511579

[18] X. Wei, W. Mei, D. Wang, B. Ning, and Z. Chen, "Joint beamforming and antenna position optimization for movable antenna-assisted spectrum sharing," *IEEE Wireless Commun. Lett.*, 2024, DOI:10.1109/LWC.2024.3421636.

[19] D. Wang, W. Mei, B. Ning, and Z. Chen, "Flexible beam coverage optimization for movable-antenna array," *arXiv preprint arXiv:2408.00434*, 2024.

[20] L. Zhu, W. Ma, Z. Xiao, and R. Zhang, "Performance analysis and optimization for movable antenna aided wideband communications," *arXiv preprint arXiv:2401.08974*, 2024.

[21] S. Dang, G. Chen, and J. P. Coon, "Lexicographic codebook design for OFDM with index modulation," *IEEE Trans. Wireless Commun.*, vol. 17, no. 12, pp. 8373–8387, Dec. 2018.

[22] S. Dang, J. P. Coon, and G. Chen, "Adaptive OFDM with index modulation for two-hop relay-assisted networks," *IEEE Trans. Wireless Commun.*, vol. 17, no. 3, pp. 1923–1936, Mar. 2018.

[23] M. Wen, X. Chen, Q. Li, E. Basar, Y.-C. Wu, and W. Zhang, "Index modulation aided subcarrier mapping for dual-hop OFDM relaying," *IEEE Trans. Commun.*, vol. 67, no. 9, pp. 6012–6024, Sep. 2019.

[24] R. Y. Mesleh, H. Haas, S. Sinanovic, C. W. Ahn, and S. Yun, "Spatial modulation," *IEEE Trans. Veh. Technol.*, vol. 57, no. 4, pp. 2228–2241, Jul. 2008.

[25] Y. Xiao, Z. Yang, L. Dan, P. Yang, L. Yin, and W. Xiang, "Low-complexity signal detection for generalized spatial modulation," *IEEE Commun. Lett*, vol. 18, no. 3, pp. 403–406, Mar. 2014.

[26] J. Li, M. Wen, X. Cheng, Y. Yan, S. Song, and M. H. Lee, "Generalized precoding-aided quadrature spatial modulation," *IEEE Trans. Veh. Technol.*, vol. 66, no. 2, pp. 1881–1886, Feb. 2017.

[27] P. Yang, Y. Xiao, M. Xiao, J. Zhu, S. Li, and W. Xiang, "Enhanced receive spatial modulation based on power allocation," *IEEE J. Sel. Top Signal Process.*, vol. 13, no. 6, pp. 1312–1325, Oct. 2019.

[28] J. Zhu, P. Yang, Y. Xiao, X. Lei, and Q. Chen, "Low RF-complexity receive spatial modulation for millimeter-wave MIMO communications," *IEEE Commun. Lett.*, vol. 22, no. 7, pp. 1338–1341, Jul. 2018.

[29] S. Gao, X. Cheng, and L. Yang, "Spatial multiplexing with limited RF chains: Generalized beamspace modulation (GBM) for mmwave massive MIMO," *IEEE J. Sel. Areas Commun.*, vol. 37, no. 9, pp. 2029–2039, Sep. 2019.

[30] X. Wang, L. Kong, F. Kong, F. Qiu, M. Xia, S. Arnon, and G. Chen, "Millimeter wave communication: A comprehensive survey," *IEEE Commun. Surveys Tuts.*, vol. 20, no. 3, pp. 1616–1653, 3rd Quart., 2018.

[31] P. Wang, J. Fang, L. Dai, and H. Li, "Joint transceiver and large intelligent surface design for massive MIMO mmWave systems," *IEEE Trans. wireless Commun.*, vol. 20, no. 2, pp. 1052–1064, Oct. 2020.

[32] M. Nemati, B. Maham, S. R. Pokhrel, and J. Choi, "Modeling RIS empowered outdoor-to-indoor communication in mmWave cellular networks," *IEEE Trans. Commun.*, vol. 69, no. 11, pp. 7837–7850, Nov. 2021.

[33] J. He, H. Wymeersch, and M. Juntti, "Channel estimation for RIS-aided mmWave MIMO systems via atomic norm minimization," *IEEE Trans. Wireless Commun.*, vol. 20, no. 9, pp. 5786–5797, Sep. 2021.

[34] M. Di Renzo, A. Zappone, M. Debbah, M.-S. Alouini, C. Yuen, J. De Rosny, and S. Tretyakov, "Smart radio environments empowered by reconfigurable intelligent surfaces: How it works, state of research, and the road ahead," *IEEE J. Sel. Areas Commun.*, vol. 38, no. 11, pp. 2450–2525, Jul. 2020.

[35] R. Li, B. Guo, M. Tao, Y.-F. Liu, and W. Yu, "Joint design of hybrid beamforming and reflection coefficients in RIS-aided mmWave MIMO systems," *IEEE Trans. Commun.*, vol. 70, no. 4, pp. 2404–2416, Apr. 2022.

[36] S. Gong, C. Xing, P. Yue, L. Zhao, and T. Q. Quek, "Hybrid analog and digital beamforming for RIS-assisted mmWave communications," *IEEE Trans. Wireless Commun.*, vol. 22, no. 3, pp. 1537–1554, Mar. 2023.

[37] R. Li, S. Sun, Y. Chen, C. Han, and M. Tao, "Ergodic achievable rate analysis and optimization of RIS-assisted millimeter-wave MIMO communication systems," *IEEE Trans. Wireless Commun.*, vol. 22, no. 2, pp. 972–985, Feb. 2023.

[38] X. Zhu, W. Chen, Z. Li, Q. Wu, Z. Zhang, K. Wang, and J. Li, "RIS-aided spatial scattering modulation for mmWave MIMO transmissions," *IEEE Trans. Commun.*, vol. 71, no. 12, pp. 7378–7392, Dec. 2023.

[39] M. Raeisi, A. Koc, I. Yildirim, E. Basar, and T. Le-Ngoc, "Cluster index modulation for reconfigurable intelligent surface-assisted mmWave massive MIMO," *IEEE Trans. Wireless Commun.*, vol. 23, no. 2, pp. 1581–1591, Feb. 2024.

[40] R. Yang, N. Wei, Z. Dong, X. Zou, Y. Li, and F. Xu, "Joint beamforming optimization for RIS enhanced mmWave communications with spatial modulation," *IEEE Commun. Lett.*, 2024, early access, DOI. 10.1109/LCOMM.2024.3368524.

[41] F. R. Ghadi, K.-K. Wong, W. K. New, H. Xu, R. Murch, and Y. Zhang, "On performance of RIS-aided fluid antenna systems," *arXiv preprint arXiv:2402.16116*, 2024.

[42] J. Chen, Y. Xiao, J. Zhu, Z. Peng, X. Lei, and P. Xiao, "Low-complexity beamforming design for RIS-assisted fluid antenna systems," in *IEEE Int. Conf. Commun. (ICC Workshops)*, pp. 1377–1382, 2024.

[43] J. Zhu, G. Chen, P. Gao, P. Xiao, Z. Lin, and A. Quddus, "Index modulation for fluid antenna-assisted MIMO communications: System design and performance analysis," *IEEE Trans. Wireless Commun.*, vol. 23, no. 8, pp. 9701–9713, Aug. 2024.

[44] J. Hu, H. Yin, and E. Björnson, "Mmwave MIMO communication with semi-passive RIS: A low-complexity channel estimation scheme," in *2021 IEEE Global Communications Conference (GLOBECOM)*, pp. 01–06, IEEE, Dec. 2021.

[45] T. Ma, Y. Xiao, X. Lei, P. Yang, X. Lei, and O. A. Dobre, "Large intelligent surface assisted wireless communications with spatial modulation and antenna selection," *IEEE J. Sel. Areas Commun.*, vol. 38, no. 11, pp. 2562–2574, Nov. 2020.

[46] Z. Xiao, S. Cao, L. Zhu, Y. Liu, B. Ning, X.-G. Xia, and R. Zhang, "Channel estimation for movable antenna communication systems: A framework based on compressed sensing," *IEEE Trans. Wireless Commun.*, vol. 23, no. 9, pp. 11814–11830, Sep. 2024.

[47] R. Zhang, L. Cheng, W. Zhang, X. Guan, Y. Cai, W. Wu, and R. Zhang, "Channel estimation for movable-antenna MIMO systems via tensor decomposition," *IEEE Wireless Commun. Lett*, Early access, 2024, DOI: 10.1109/LWC.2024.3450592.

[48] B. Pan, J. Papapolymerou, and M. M. Tentzeris, "MEMS integrated and micromachined antenna elements, arrays, and feeding networks," *Modern Antenna Handbook*, pp. 829–865, 2008.

[49] L. Jing, M. Li, and R. Murch, "Compact pattern reconfigurable pixel antenna with diagonal pixel connections," *IEEE Trans. Antennas Propag.*, vol. 70, no. 10, pp. 8951–8961, Oct. 2022.

[50] A. Koc and T. Le-Ngoc, "Full-duplex mmWave massive MIMO systems: A joint hybrid precoding/combining and self-interference cancellation design," *IEEE Open J. Commun. Soc.*, vol. 2, pp. 754–774, 2021.

[51] S. Guo, S. Lv, H. Zhang, J. Ye, and P. Zhang, "Reflecting modulation," *IEEE J. Sel. Areas Commun.*, vol. 38, no. 11, pp. 2548–2561, Nov. 2020.

[52] M. K. Simon and M.-S. Alouini, *Digital Communication over Fading Channels*, vol. 86. John Wiley & Sons, 2004.

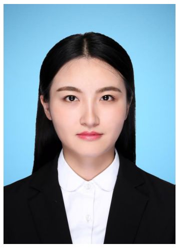

Jing Zhu (Member, IEEE) received the B.S and M.S. degree from the University of Electronic Science and Technology of China (UESTC), Chengdu, China, in 2016 and 2019, respectively, and the Ph.D. degree from the University of Surrey, U.K., in 2023. Her research interests include index modulation, flexible electronics, fluid antenna systems, RIS and massive MIMO.

Qu Luo (Member, IEEE) received the Ph.D. degree from the University of Surrey, U.K., in 2024. He is currently a Research Fellow of wireless communications with 5GIC/6GIC, Institute for Communication Systems, University of Surrey. Prior to this, he was with Huawei Technologies Company Ltd., Chengdu, China, from 2019 to 2020. He was a Visiting Collaborative Researcher with the University of Essex in 2023. His research interests include proof-of-concept physical layer design, joint sensing and communication, non-orthogonal multiple access, random access, deep/machine learning in the physical layer, and joint MAC layer and physical layer optimization. He was a recipient of the Exemplary Reviewer Awards of IEEE WIRELESS COMMUNICATION LETTERS from 2020 to 2023 and IEEE COMMUNICATION LETTERS from 2022 to 2023 and the Best Paper Awards of the IEEE CSPS in 2018 and the IWCMC in 2024.

Gaojie Chen (S'09 – M'12 – SM'18) received the B.Eng. and B.Ec. Degrees in electrical information engineering and international economics and trade from Northwest University, China, in 2006, and the M.Sc. (Hons.) and PhD degrees in electrical and electronic engineering from Loughborough University, Loughborough, U.K., in 2008 and 2012, respectively. After graduation, he took up academic and research positions at DT Mobile, Loughborough University, University of Surrey, University of Oxford and University of Leicester, U.K. He is currently a Professor and Associate Dean of the School of Flexible Electronics (SoFE), Sun Yat-sen University, China. His current research interests include wireless communications, flexible electronics, satellite communications, the Internet of Things and secrecy communications. He received the Best Paper Awards from the IEEE IECON 2023, and the Exemplary Reviewer Awards of the IEEE WIRELESS COMMUNICATIONS LETTERS in 2018, the IEEE TRANSACTIONS ON COMMUNICATIONS in 2019 and the IEEE COMMUNICATIONS LETTERS in 2020 and 2021; and Exemplary Editor Awards of the IEEE COMMUNICATIONS LETTERS and IEEE WIRELESS COMMUNICATIONS LETTERS in 2021, 2022 and 2023, respectively. He served as an Associate Editor for the IEEE JOURNAL ON SELECTED AREAS IN COMMUNICATIONS - MACHINE LEARNING IN COMMUNICATIONS from 2021-2022. He serves as an Editor for the IEEE TRANSACTIONS ON WIRELESS COMMUNICATIONS, IEEE TRANSACTIONS ON COGNITIVE COMMUNICATIONS NETWORKING, IEEE WIRELESS COMMUNICATIONS LETTERS, and a Senior Editor for the IEEE COMMUNICATIONS LETTERS, and a Panel Member of the Royal Society's International Exchanges, UK.

Pei Xiao (Senior Member, IEEE) is currently a Professor of wireless communications with the Institute for Communication Systems (ICS), University of Surrey. He is also the Technical Manager of 5GIC/6GIC, leading the research team in the new physical layer work area and coordinating/supervising research activities across all the work areas (https://www.surrey.ac.uk/institute-communicationsystems/5g-6g-innovation-centre). Prior to this, he was with Newcastle University and Queen's University Belfast. He also held positions at Nokia Networks, Finland. He has published extensively in the fields of communication theory, RF and antenna design, and signal processing for wireless communications. He is an inventor of over 15 recent patents addressing bottleneck problems in 5G/6G system.

Yue Xiao (Member, IEEE) received the Ph.D degree in communication and information systems from the University of Electronic Science and Technology of China (UESTC) in 2007. He is currently a Professor with National Key Laboratory of Wireless Communications, UESTC. He has published more than 100 international journals and has been in charge of more than 20 projects in the area of Chinese 3G/4G/5G wireless communication systems. He is an inventor of more than 50 Chinese and PCT patents on wireless systems. His research interests are in system design and signal processing toward future wireless communication systems. He currently serves as a Senior Associate Editor of IEEE COMMUNICATIONS LETTERS and Associate Editor of IEEE OPEN JOURNAL OF THE COMMUNICATIONS SOCIETY.

Kai-Kit Wong (M'01-SM'08-F'16) received the BEng, the MPhil, and the PhD degrees, all in Electrical and Electronic Engineering, from the Hong Kong University of Science and Technology, Hong Kong, in 1996, 1998, and 2001, respectively. After graduation, he took up academic and research positions at the University of Hong Kong, Lucent Technologies, Bell-Labs, Holmdel, the Smart Antennas Research Group of Stanford University, and the University of Hull, UK. He is Chair in Wireless Communications at the Department of Electronic and Electrical Engineering, University College London, UK. His current research centers around 6G and beyond mobile communications. He is Fellow of IEEE and IET. He served as the Editor-in-Chief for IEEE WIRELESS COMMUNICATIONS LETTERS between 2020 and 2023.